Received: 8 August 2022 | Revised: 3 November 2022 | Accepted: 19 November 2022

DOI: 10.1002/jcc.27050

RESEARCH ARTICLE

Journal of COMPUTATIONAL CHEMISTRY WILEY

Large scale peptide screening against main protease of SARS CoV-2

Md. Jaish Uddin[1] | Hasina Akhter[1] | Urmi Chowdhury[1] | Jannatul Mawah[1] | Sanzida Tul Karim[1] | Mohammad Jomel[1] | Md. Sirajul Islam[1] | Mohammad Raqibul Islam[1] | Latifa Afrin Bhuiyan Onin[1] | Md. Ackas Ali[1,2] | Faiyaz Md. Efaz[1] | Mohammad A. Halim[2]

[1]Division of Infectious Disease and Division of Computer-Aided Drug Design, The Red-Green Research Centre, Dhaka, Bangladesh

[2]Department of Chemistry and Biochemistry, Kennesaw State University, Kennesaw, Georgia, USA

Correspondence
Mohammad A. Halim, Department of Chemistry and Biochemistry, Kennesaw State University, Kennesaw, GA, USA.
Email: mhalim1@kennesaw.edu

Abstract

The COVID-19 pandemic has been a public health emergency, with deadly forms constantly emerging around the world, highlighting the dire need for highly effective antiviral therapeutics. Peptide therapeutics show significant potential for this viral disease due to their efficiency, safety, and specificity. Here, two thousand seven hundred eight antibacterial peptides were screened computationally targeting the Main protease (Mpro) of SARS CoV-2. Six top-ranked peptides according to their binding scores, binding pose were investigated by molecular dynamics to explore the interaction and binding behavior of peptide-Mpro complexes. The structural and energetic characteristics of Mpro-DRAMP01760 and Mpro-DRAMP01808 complexes fluctuated less during a 250 ns MD simulation. In addition, three peptides (DRAMP01760, DRAMP01808, and DRAMP01342) bind strongly to Mpro protein, according to the free energy landscape and principal component analysis. Peptide helicity and secondary structure analysis are in agreement with our findings. Interaction analysis of protein-peptide complexes demonstrated that Mpro's residue CYS145, HIS41, PRO168, GLU166, GLN189, ASN142, MET49, and THR26 play significant contributions in peptide-protein attachment. Binding free energy analysis (MM-PBSA) demonstrated the energy profile of interacting residues of Mpro in peptide-Mpro complexes. To summarize, the peptides DRAMP01808 and DRAMP01760 may be highly Mpro specific, resulting disruption in a viral replication and transcription. The results of this research are expected to assist future research toward the development of antiviral peptide-based therapeutics for Covid-19 treatment.

KEYWORDS
antibacterial peptide, free energy landscape, helicity, main protease, MM-PBSA, SARS CoV-2

1 | INTRODUCTION

Since the beginning of the SARS-CoV-2 pandemic, approximately 5 million people have died and 418 million have been infected around the world.[1] In case of severity, this disease's clinical characteristics get intense causing pneumonia, major dysfunction in kidney, severe acute respiratory symptoms and even death.[2] The availability of therapeutic medications that can be used to treat acutely infected patients is quite limited, despite the fact that authorized vaccinations provide highly effective prophylactic protection against the beginning of the

 © 2022 Wiley Periodicals LLC.

disease.[3,4] Nonetheless, its effectiveness in treating COVID-19 individuals is questionable due to the virus be highly mutation prone. As a result, there is a pressing need to develop drugs that are highly selective and have few adverse effects when used against viral targets.

The main protease (Mpro) of coronaviruses is one of the most-studied therapeutic targets,[5] belonging to 16 nonstructural proteins (NSPs) of coronavirus (CoV). Mpro is important to process the polyproteins that are encoded from the viral RNA with the papain-like protease.[6,7] The structure of the SARS-CoV-2 main protease is nearly identical to SARS-CoV ortholog (96% identity) and furthermore, all of the key residues involved in catalysis, binding and dimerization are entirely conserved.[8] SARS-CoV-2 Mpro is a homodimer protein that consists of two nearly perpendicular monomers.[9] Each monomer has three domains and a catalytic dyad (HIS41 and CYS145) located in a cleft between domain I (residues 10–99) and domain II (residues100–182). Domain I and II residues create the six-stranded antiparallel β barrel structure with 4 subsites (S1, S2, S3, and S4).[5] A long loop connects the catalytic domains to the C-terminal domain III (residues 198–303), which is made up of 5 antiparallel α-helices. The Mpro has 11 cleaving sites to cleave large polyprotein 1ab (replicase 1 ab∼790 kDa).[10,11] The substrate and Mpro cleavage occur between GLN in P1 position and a GLY/ALA/SER in P1′ position (P and P′ indicate the residues before and after the scissile bond, respectively) where the presence of GLN is necessary.[8] Cysteine proteases reaction mechanism follows two basic steps.[8] In the 1st step of Acylation, acyl–enzyme complex is formed by the breakdown of peptide bond and releasing the P′ fragment of substrate where CYS145 is bound to the carbon atom covalently with P1 residues of target protein. In the 2nd step of Deacylation, the acyl–enzyme complex is electrolyzed and releases the P fragment to recover the enzymatic active site. Covalent inhibitors of acyl–enzyme complexes remain bonded with the active site that cannot be electrolyzed.[12,13] Previous study reported that, inhibitors targeting SARS-CoV Mpro may also reduce SARS-CoV-2 Mpro's enzymatic activity.[14] By inhibiting Mpro function, the virus's replication may be effectively stopped. The inhibitors against Mpro are less harmful because no human proteases with a similar cleavage selectivity have been identified.[15]

Recently, Pfizer developed a small molecule drug (PF-07321332) to inhibit the main protease which is responsible for viral replication. The drug, PF-07321332, can be taken orally, has good selectivity and safety profiles, and prevents infection in a mouse model.[16] The Pfizer-developed drug has been approved for use in emergency situations following promising results from phase 3 clinical studies for the treatment of COVID-19.[17] According to other research, PF-00835231, which was thought to be an effective SARS CoV-1 inhibitor, may also work well against SARS Cov-2 Mpro due to their high rate of sequence similarity.[16,17] However, small molecule drugs usually have adverse off-target effects and, following prolonged administration may result in treatment resistance. In contrast, peptide therapeutics holds considerable potential for the treatment of SARS-CoV-2 illness. In 1922, the first medical use of insulin generated from animal pancreases was established, and the field of peptide treatments was formed.[18] Peptides are well tolerated and safe for having less system toxicity and lower off-target side effects which make them distinct to other traditional small molecules or synthetic compounds.[19] In addition, they have high selectivity and efficacy allowing them to interact with any specific cell surface receptors.[20] Peptides with antimicrobial activity are amphiphilic, cationic molecules ranging from 10 to 50 amino acids, show a considerable ability to combat harmful microorganisms like bacteria, virus, and fungi.[21,22] Antimicrobial peptides (AMPs) are considered as one of the key components of innate immune system that comprises the first-line defense against invading pathogens.[23] The positively charged residues of AMPs and its hydrophobic amino acids allow them to bind electrostatically with negatively charged cell surface, resulting in breakdown of target pathogenic cells.[21] They grab attention due to their significant pharmacological profiles like high potency and biocompatibility, low accumulation of tissues, discoverability at peptide or nucleic acid levels.[24] Despite having all of these advantages, the application of peptide therapeutics has some limitation for their lability to serum proteases, high clearance, low oral bioavailability, poor membrane permeability and solubility.[24,25] Currently, there are about 80 peptide medications available, with more than 150 peptides in clinical development and another 400–600 peptides in preclinical trials.[18,20,26] Furthermore, the cyclic peptide inhibitor was developed by Kreutzer et al. with higher proteolytic stability and membrane permeability than their linear counterparts against Mpro.[27] Therefore, peptides have a great potential as therapeutics of SARS-CoV-2.

Despite multiple initiatives underway to develop potential therapeutics, there is no specific efficient treatment available for COVID 19.[28,29] The traditional drug development process widely considered as time-consuming and expensive with a success rate of only 2.01%.[30] On the Contrary to the de-novo drug development approach, drug repurposing is a very effective strategy as it encompasses less time and cost to locate a therapeutic agent.[30,31] As a result, discovering novel therapeutics for this deadly virus will need a comprehensive approach to drug repositioning. Since the launch of Covid-19, several FDA-approved medications have been clinically trialed, including remdesivir, ribavirin, lopinavir, favipiravir, ritonavir, darunavir, arbidol, chloroquine, tocilizumab, hydroxychloroquine, and interferons.[30] However, the majority of these drugs have only made a limited effort to combat the pandemic.[32] Nonetheless, due to the lack of high efficacious medicines and the intensity of the current health crisis, quick identification approaches for preventive and therapeutic tactics should be investigated from all angles.[32] Previously, our lab has executed several computational investigations on peptide therapeutics against numerous infectious proteins of SARS-CoV-2.[33–35]

In this study, we computationally screened two thousand seven hundred eight antibacterial peptides against Mpro of SARS-CoV-2. A high affinity Mpro protein binders were identified and potential interaction pathways for peptides with a greater Mpro-protein binding affinity were investigated using molecular dynamics simulation (MD).

2 | MATERIALS AND METHODS

2.1 | Molecular docking and interaction

A total of two thousand seven hundred eight antibacterial peptides were selected from the DRAMP database.[36,37] Pep-fold 3.5 was used to model all of the peptides by setting number of simulation 200.[38,39] The crystal structure of SARS-CoV2 Mpro (PDB ID: 6Y2G) was retrieved with a resolution of 2.20 Å from the RCSB Protein Data Bank (PDB).[5] All the undesirable ligands and water molecules were removed. The PatchDock server[40] was used to perform molecular docking of predicted antibacterial peptides to Mpro, with active site residues being emphasized. FireDock refined the preliminary 1000 peptide–Mpro complexes obtained through PatchDock.[41] MD simulation was used to examine the top six ranked peptide-Mpro complexes based on their binding affinity, sequence length (ranges between 13 and 20) and binding posture.

To check the efficacy of our screening procedure, random decoy data sets of the top six peptides are generated using an in-house Python script. Pepfold3.5 was used to model random decoy data sets of the top six peptides.[38,39] The same binding site mentioned earlier was taken into account when modeled sets were docked against Mpro SARS CoV-2 in PatchDock.[40]

2.2 | Molecular dynamics (MD) simulations

In this investigation, Molecular dynamics simulation was performed on apo-Mpro, and six selected peptides (based on higher binding energy, peptide length and binding poses) DRAMP01342, DRAMP01737, DRAMP01760, DRAMP01771, DRAMP01808, and DRAMP18658 bound to Mpro complex. To solvate the system, a TIP3P[42] water model with 10 Å of buffer distance was employed. In order to neutralize the system, 0.15 M of NaCl and Na^+ ions were added to each of the system. The OPLS2005 force field was employed in each of the systems. The entire atom based MD simulation of the system was carried out with the help of Desmond dynamic suite.[43] The system was simulated using the NPT ensemble. The parameters that have been taken into consideration were a constant number of particles, 1 bar of pressure and 310 K temperature. To satisfy the constraints geometry of hydrogen bonds, the M-SHAKE[44] algorithm was used. This enabled 2.0 fs time steps to be performed while the simulation was running. Long-range electrostatic interactions were applied with periodic boundary conditions by using the k-space Gaussian split Ewald method[45] and van der Waals (VDW) cut-off was set to 9 Å based on a uniform density approximation. For non-bonded short-range interactions, cut-off distance of 9 Å were considered which was determined by an r-RESPA integrator.[46] In every 2 and 6 fs respectively, the short-range and the long-range forces were updated. The MD simulation with a time of 250 ns was carried out and the trajectories had been recorded at interval of every 100 ps to assess the trajectory data. Considering the Root-mean-square deviation (RMSD), root-mean-square fluctuation (RMSF), radius of gyration (Rg), solvent accessible surface area (SASA) which were obtained from the MD simulations, allowing for analysis of the dynamic nature and structural changes of the complexes Secondary structure of protein was analyzed by DSSP program.[47]

2.3 | Free energy landscape

The free energy landscape (FEL) estimates and tracks all the conformational flexibility and associated with energy levels of a certain system during a defined time scale. The energy is regarded as Gibb's free energy, which was determined by using protein entropy and enthalpy.[48] The following equation was used for calculating the Gibb's free energy:

$$Gi = -K_B T \ln\left(\frac{N_i}{N_{max}}\right)$$

Here, K_B stands for the Boltzmann's constant, T denotes temperature, N_i for the population in bin i and N_{max} is the population in bin with the highest density. Geo-Measure plugin was incorporated to produce FEL plot. In this case, root- mean square deviation (RMSD) and radius of gyration (Rg) were used to describe the FEL.[49]

2.4 | Principal component analysis

Principal component analysis (PCA) is a multidimensional data reduction method where structural and energy profiles of the MD data were analyzed. Here, we predicted similarities and dissimilarities of structural and energy profiles of protein-peptide complexes.[50,51] Various multivariate factors such as bond distance, bond angle, dihedral angle, coulomb, and van der Waal's energy were analyzed to find dissimilarities among various energy and structural profiles of protein-peptide complexes.[52] The analysis was based on the following model:

$$X = T_K P_K^T + E$$

Here X matrix is reduced to a product of the two new matrices T_K and $P_K.T_K$is a matrix of score describing relationship between samples. P_K is a matrix of loading which describes variables related to each other whereas K and E are number of factor and residual matrix respectively. The last 100 ns of MD data of six selected protein-peptide complexes were used for PCA analysis.

2.5 | Binding free energy analysis of interacting residues

The Molecular Mechanics Poisson–Boltzmann Surface Area continuum solvation (MM-PBSA) is a consistently used and widely-adopted method for evaluating protein-inhibitor affinity. The approach is frequently employed to determine the binding affinities and hot spots, as well as to assess structural integrity.[53–55] Furthermore, MM-PBSA enables the analysis of contributions from individual protein-ligand

residues, providing precise information on the energetic contributions made by each residue to the binding system and identifying the major binding interactions.[56,57] Binding free energies (ΔG_{Bind}) followed by per-residue energy contributions of the Mpro–Peptide complexes were calculated from MM-PBSA evaluated by Adaptive Poisson–Boltzmann Solver using the g_mmpbsa package.[58]

The protein's binding free energy with a ligand in a continuum solvent can be expressed generally as,

$$\Delta G_{binding} = G_{complex} - \left(G_{protein} + G_{ligand}\right)$$

Where, $G_{complex}$ is the total free energy of the protein-ligand complex and $G_{protein}$ and G_{ligand} are the total free energies of the isolated protein and ligand in a solvent, respectively. The free energy of binding ΔG_{bind} for the isolated protein−ligand complex is evaluated as follows:

$$G = E_{bonded} + E_{el} + E_{vdw} + G_{polar} + G_{nonpolar} - TS$$

In the second equation, E_{bonded} is the bonded, E_{el} is the electrostatic and E_{vdw} is the Van der Waals energy component from the MM force field in a vacuum. In the single trajectory approach, the conformation of protein and ligand in the bound and unbound forms are assumed to be identical. Thus ΔE_{bonded} is always taken as zero. G_{polar} is the polar solvation energy component which is calculated by using the approximation for solving the Poisson-Boltzmann (PB) equation. $G_{nonpolar}$ is the nonpolar solvation energy contribution and is estimated using a linear approximation including the solvent-accessible surface area (SASA). Finally, TS refers to the entropic contribution to the free energy in a vacuum where T and S denote the temperature and entropy respectively. TS is ignored in this study as the change of this term does not affect the relative binding energy of ligands.[59] In the current investigation, the MMPBSA binding free energies were determined using precise snapshots of the last 100 ns of MD trajectory data taken at 100 ps intervals. Here dielectric constant employed for vacuum (vdie), solute (pdie) and solvent (sdie) are 1, 2, and 80 respectively and the solvent probe radius is 1.4 Å. SASA has been selected as our nonpolar model for its widely acceptance and accuracy.[60,61] Surface tension constant (c) was taken at 0.0226778 kJ/mol. $Å^2$ and the SASA constant was also taken at 3.84928 kJ/mol for fitting. Finally, Residue-specific contributions toward binding were obtained from the MmPbSaDecomp.py program.

3 | RESULT AND DISCUSSION

3.1 | Molecular docking and interaction

A total of two thousand seven hundred eight antibacterial peptides were docked against Main protease (Mpro) of SARS-CoV2; maintaining the specified binding site composed of residues which include HIS41, MET49, PHE140, GLY143, SER144, CYS145, HIS163, HIS164, GLU166, PRO168, and GLN189. Docking results of two thousand seven hundred eight peptides against Mpro were enlisted in Table S1. Table S2 summarizes the amino acid sequence, length, and pharmacological information of peptides. The binding affinities of two thousand seven hundred eight peptides, ranging from −79.91 to −18.83 kcal/mol, are summarized in Figure 1A. Among all peptide-Mpro complexes, the majority had binding affinity ranging between −49.91 to −39.91 kcal/mol (Figure 1A). Table 1 illustrates the docking results of the top 50 peptides. However, DRAMP03616, DRAMP03734, DRAMP01365, and DRAMP03457 had a higher binding affinity but drifted away from the binding pocket of protein. Mpro residues CYS145, HIS41, MET49, PRO168, and GLU166 interacted highly with peptides in a nonbonded way (Figure 1B). In addition, PRO168 and GLU166 were shown to interact with several antibacterial peptides (Figure 1C), denoting that these residues are significant for peptide attachment.[62,63] Dimerization of the enzyme is required for catalytic activity as the N-finger of both protomers interacts with GLU166 in a reciprocal manner.[5] Furthermore, it has also been reported that the mutation of GLU166 in SARS-CoV-2 Mpro could modify inhibitors affinity.[63] Therefore, the residue GLU166 may play crucial role in inhibitor's binding to SARS-CoV-2 Mpro, which could be a potential research target.[63] This evidence points to our docking results having a favorable impact. In the interaction between peptide and Mpro, the hydrogen bond interaction was significant, accounting for 51% of all interactions (Figure 1D). Apart from hydrophobic bond interaction which contributed to 43%, while electrostatic interactions made up only 6% of all interactions. Based on the length of sequence, binding pose and nonbonding interaction DRAMP01760, DRAMP01808, DRAMP18658, DRAMP01342, DRAMP01737, DRAMP01771 were chosen as the most potential candidates of SARS-CoV-2 Mpro to continue further investigation.

The docking nonbonded interaction of decoy datasets are listed in Table S3. The analysis of each Mpro-decoy complex showed that critical residues interacted at a high rate, with CYS145 having the greatest interaction rate of almost 25% and acting as the SARS COV-2 Mpro's most important residue. In addition, other significant residues such as MET49, HIS41, GLU166, and PRO168 interacted with model peptides at rates of 21.9%, 16.9%, 11.8%, and 10%, respectively. These data demonstrate the consistency of our findings and categorically support the docking interactions of the top six peptides (DRAMP01760, DRAMP01808, DRAMP18658, DRAMP01342, DRAMP01737, DRAMP01771).

3.2 | Molecular dynamics (MD) simulations

Molecular dynamics simulations were performed by Desmond dynamic suite to analyze the periodic evolution of the Mpro-peptides[64] covering a time limit of 250 ns for each complex. The post simulation trajectories were assessed considering a general analysis which incorporates RMSD,[65] Rg,[66] SASA, RMSF.

The RMSD metric of the initial structure and the average simulated structure of all MD trajectory frames can be used to gain insight into the resolution of simulated protein–ligand complexes. On average, the Protein-ligand RMSDs of both the Mpro and the complexes depicted in Figure 2A fluctuated between values ranging from 1.62 to

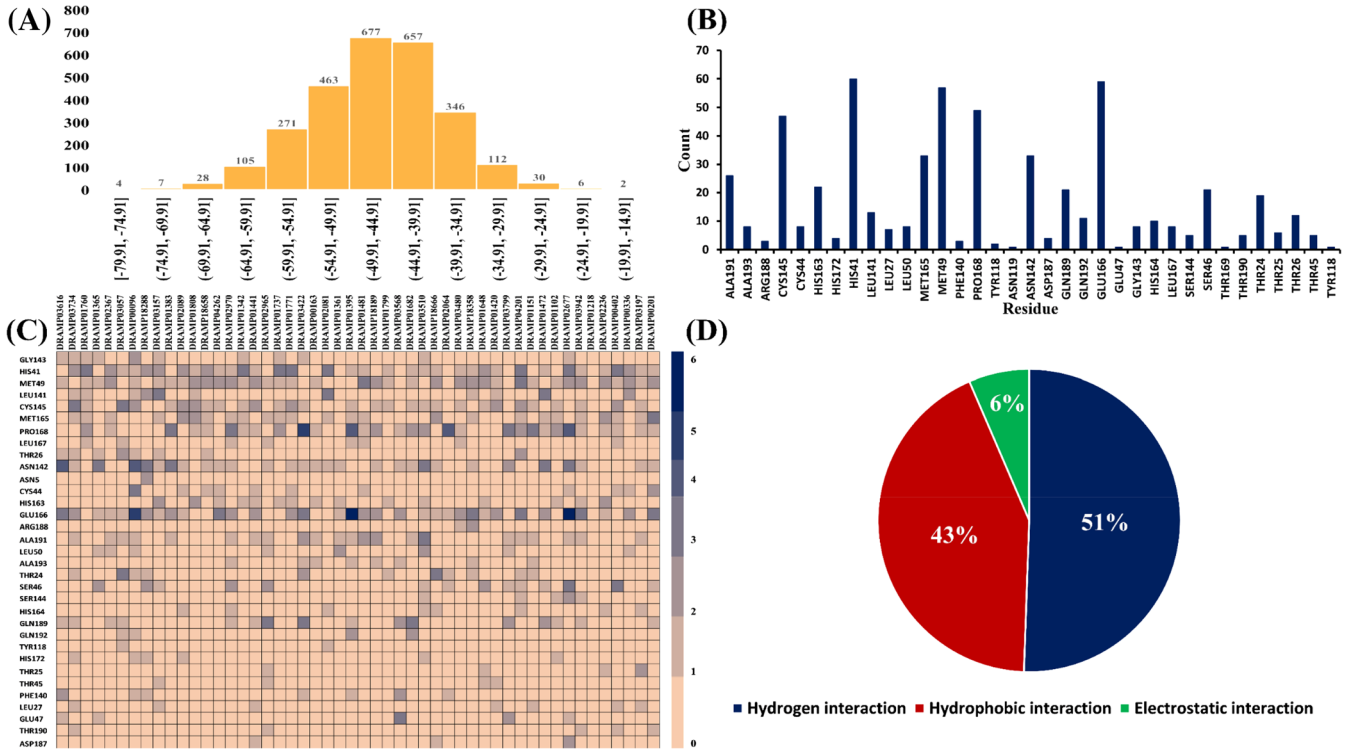

FIGURE 1 (A) All antibacterial peptide's frequency distribution over a range of docking scores; (B) Interacting residues of SARS-Cov2 Mpro; (C) Residue–residue interaction map for top 50 peptide–Mpro complexes; (D) Distribution of nonbonded interactions of protein peptide complexes

2.59 Å. While Mpro (mean 1.62 Å), Mpro-DRAMP018658 (mean 1.69 Å) and Mpro-DRAMP01737 (mean 1.79 Å) remained most stable among the other complexes during the simulation period. Smaller fluctuation in RMSD reveals strong stability in Protein ligand binding.[67] In case of Mpro-DRAMP01771, the RMSD pattern demonstrates a dramatic fall at 44.60 ns and a drastic upward turn at 245 ns with a peak of 3.31 Å which happened because the complex showed its best conformational stability at 44.60 ns and with a gradual deformation till the end. Surprisingly, though the protein-ligand RMSDs of Mpro-DRAMP01808, Mpro-DRAMP01760, and Mpro-DRAMP01342 initially exhibited a twisted pattern till 54 ns with Mpro-DRAMP01760 holding a higher value of 3 Å at 31 ns representing a huge flexibility due to the random movement of the bonded peptide (Figure 3). However, after 88 ns comparing with the all the other complexes Mpro-DRAMP01342 revealed the highest distortion with an average RMSD value of 2.59 Å. Supporting the RMSD values the population density curves for Mpro and the complexes appeared quite heterogenic to each other. Moreover, Mpro-DRAMP01342 has the most different density curve proportioning to its highest conformational instability throughout the simulation time. On the other hand, the Mpro and Mpro-DRAMP018658 displayed almost similar curves with different modes and means supporting their most stable trends in terms of the RMSD values.

The peptide RMSD trends (Figure 2B), followed the pattern ranging from 4.54 to 2.23 Å. Furthermore, Mpro-DRAMP01808 has least flexibility pattern with a population consistency ranging from 1 to 3 Å. Though Mpro-DRAMP01771 originally expressed an increasing drift, with the course of time ended into a homogeneity along with the Mpro-DRAMP01760, Mpro-DRAMP018658, and Mpro-DRAMP01737 disclosing a moderate stability from roughly 5 ns to the end. Interestingly, the evident alterations between the protein domains and the peptide made the RMSD value of Mpro-DRAMP01737 take two different upward movements at 152 and 249 ns (approx.). Most importantly, Mpro-DRAMP01342 manifested a moderately stable RMSD up to 80 ns but after that a huge conformational disruption was portrayed in the graph with an average of 4.54 Å continuing till the end. The dense population around the thin line of Mpro-DRAMP01342 complex within 5 to 6 Å endorses the observation. Over all, the variation of Peptide RMSD values was caused by a change in peptide structure.

To evaluate the configurational compactness of Proteins, Radius of gyration is recommended as a formidable system.[68] The small Rg values are harmonious to a tighter packing of atoms or vice versa. Throughout the simulation, (Figure 2C) the Mpro and other Mpro-Peptide complexes exhibited almost similar type of unimodal violin plots in terms of Rg values holding discrete average values.[68] The Mpro-DRAMP01342 took a sudden upward direction reaching up to 22.75 Å at 48 ns and then fluctuated a bit till 53 ns which suggested that the complex showed a weak structural compaction initially. The average Rg values for Mpro, Mpro-DRAMP01760, Mpro-DRAMP01808, Mpro-DRAMP018658, Mpro-DRAMP01737, Mpro-DRAMP01771 were calculated as 22.1, 22.30, 22.25, 22.20, and 22.35 Å respectively from the trajectory.

Solvent accessible surface area was computed to determine the variations in the accessibility of protein to solvent.[69] A higher SASA

TABLE 1 Docking results of 50 selected peptides with higher affinity for the SARS CoV-2 Mpro.

Peptide ID	Global energy	Solution number
DRAMP03616	−79.91	359
DRAMP03734	−76.56	214
DRAMP01760	−75.18	95
DRAMP01365	−75.15	3
DRAMP02367	−74.23	2
DRAMP03057	−73.1	2
DRAMP00096	−71.66	2
DRAMP18288	−70.91	354
DRAMP03157	−70.82	1
DRAMP01383	−70.5	201
DRAMP02089	−70.3	35
DRAMP01808	−69.69	14
DRAMP18658	−69.63	1
DRAMP04262	−38.3	9
DRAMP02970	−68.79	136
DRAMP01342	−68.74	324
DRAMP01441	−68.47	43
DRAMP02965	−67.84	349
DRAMP01737	−67.82	8
DRAMP01771	−67.82	3
DRAMP03422	−67.6	41
DRAMP00163	−67.53	2
DRAMP02081	−67.23	28
DRAMP01361	−51.34	18
DRAMP01395	−66.62	2
DRAMP01481	−66.58	38
DRAMP18189	−66.33	3
DRAMP01799	−65.84	302
DRAMP03568	−65.69	340
DRAMP01682	−65.61	7
DRAMP03510	−65.56	21
DRAMP18666	−65.51	10
DRAMP02064	−65.37	306
DRAMP03480	−65.32	13
DRAMP18358	−65.26	260
DRAMP01648	−65.24	184
DRAMP01420	−65.05	61
DRAMP03799	−64.98	2
DRAMP04201	−64.94	1
DRAMP01151	−64.92	6
DRAMP01472	−64.91	74
DRAMP01102	−64.82	22
DRAMP02677	−64.45	304
DRAMP03942	−64.4	61
DRAMP01218	−64.3	94
DRAMP02236	−64.26	71
DRAMP00402	−64.21	131
DRAMP00336	−64.08	27
DRAMP03197	−64.04	29
DRAMP00201	−63.99	44

frequency denotes the more accessibility of solvents at the surface area.[34] Figure 2D demonstrated that the Mpro had the highest SASA value (14800 Å^2) implementing the fact that it holds the most expanded surface area consisting of 301 residues having different polar, positive and negative properties which attracts water molecules recognizing the finding of this study. As for the complexes, the peptides appeared to be mostly hydrophobic but among them Mpro-DRAMP01771 represented the highest SASA score (with median 14048 Å^2). Though peptide DRAMP01771 has polar and positive residues covered 23.08% of its total structure with the least presence of non-polar residues (61.54%) which supports its highest SASA consistency among other complexes. Stevens and Arkin observed that hydrophobic residues exhibit low accessibility while polar residues were found to exhibit higher accessibilities.[70] Ironically, while in terms of Protein-peptide complex's RMSD, Ligand RMSD, Rg calculation, the complex Mpro-DRAMP01342 seemed to have a highest pattern, for SASA it presented a lowest consistency (average 13828 Å^2) plot, the presence of residues with high hydrophobicity (PHE, LEU, ILE, VAL) and smaller number of polar residues in its peptide sequence supports the finding. In addition, it was noticeable that DRAMP01342 and DRAMP018658 had more than 90% structure similarity, the complex Mpro-DRAMP018658 had lower SASA score compared to Mpro-DRAMP01342. It might be because the hydrophobicity of residues is found to be correlated with the average area the residue covers upon folding.[71] This observation implies that the Mpro and the Mpro-DRAMP01771 have the highest exposure to the water solvent as compared to the other complexes.

Root mean square fluctuations can be used to explain the protein area that fluctuates throughout the simulation. Smaller conformational deviation results in the lower RMSF values. RMSD and RMSF stabilities were found to be critical in referring strong binding affinities by several research groups.[72,73] RMSF analysis of MD trajectories revealed regions with enhanced flexibility in all proteins-peptide investigated. Figure 2E displayed that the amino acid residues SER1 to ARG4 of Mpro and other Mpro-peptide complexes exhibited higher RMSF values ranging from an average of 4.4 to 1.4 Å. These residues appeared to present in the loop regions of the main protease where the occurring tendency of molecular oscillation remains at its highest. Interestingly, among all the protein and complexes Mpro-DRAMP01737 earned the highest RMSF values due to random

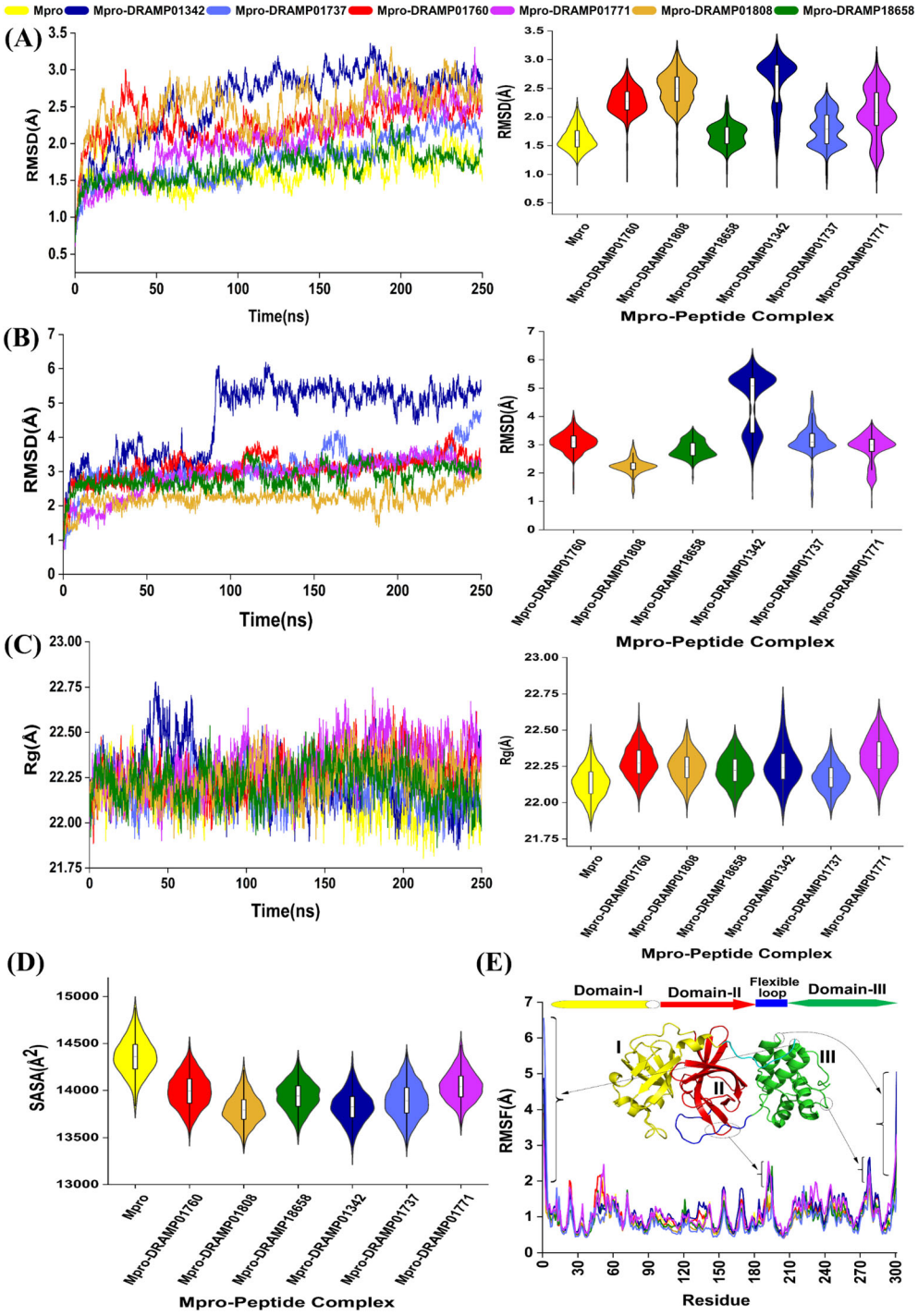

FIGURE 2 (A) Protein-peptide root-mean-square deviation (RMSD); (B) Peptide RMSD; (C) Radius of gyration (Rg); (D) Solvent accessible surface area (SASA); (E) Root-mean-square fluctuation (RMSF)

movement of several loop, coil regions. In addition, the RMSF value also showed different increasing trend for residues 193, 277, 302 and those are also found to be in the flexible loop regions between the Domain II and Domain III of the main protease. Furthermore, Kumari et al., also depicted similar type of loop regional vibration of residues in main protease.[74] To sum up, The C and N-terminal of Mpro displayed more flexibility with high RMSF fluctuation comparing to the other residues ranging from the number 6 to 290 showed more rigidity and formidability with lower RMSF values.[75]

3.3 | Intermolecular contacts of protein-peptide complexes in MD simulations

The role of key amino acids on the binding mode of peptide-protein complexes was investigated using 250 ns MD simulation snapshots for six complexes. Figure 4 shows the different types of intermolecular interactions that peptides can develop with Mpro, such as hydrogen bonds, hydrophobic interactions and water bridges.

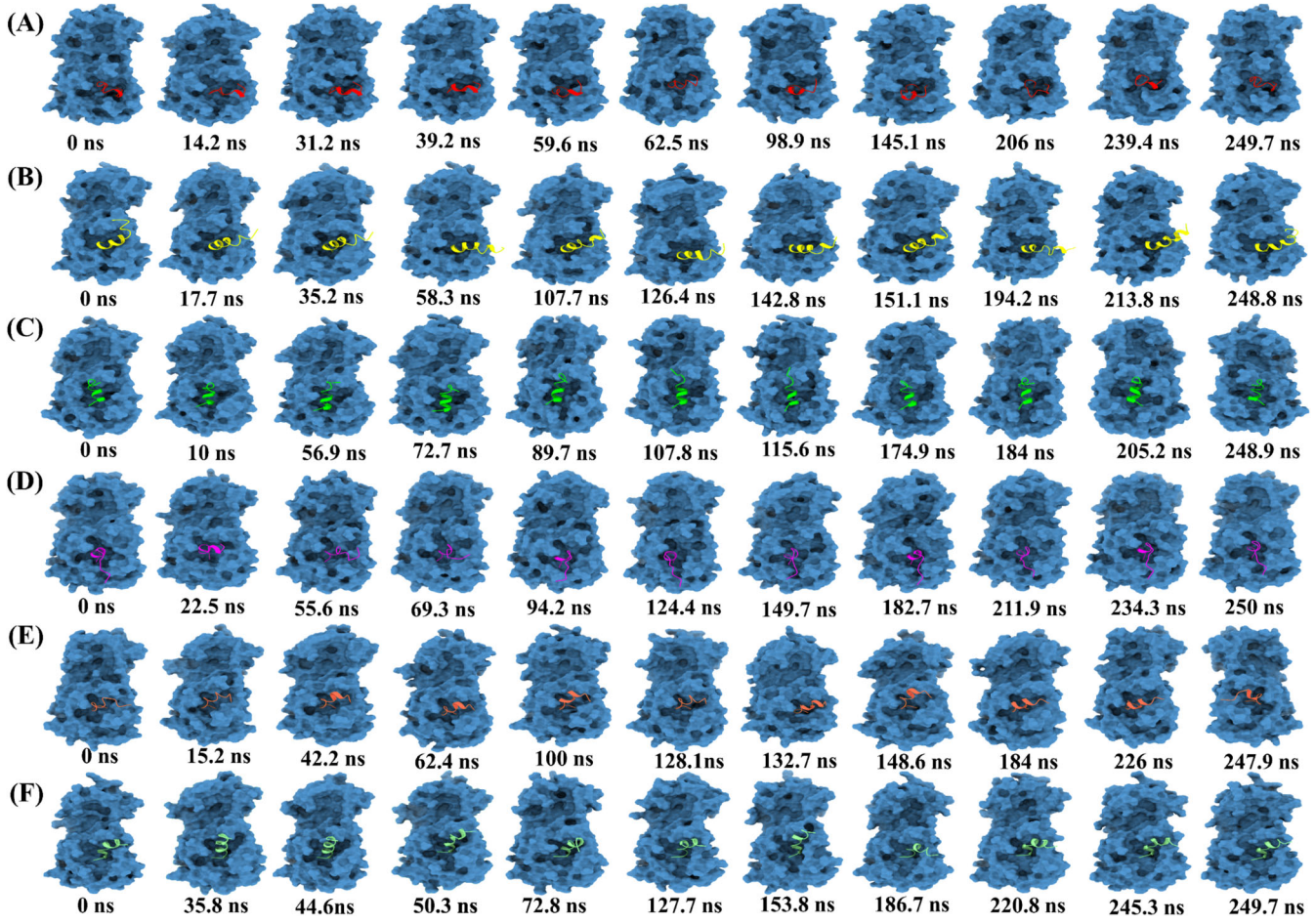

FIGURE 3 Representative snapshots during simulation. (A) Mpro-DRAMP01760; (B) Mpro-DRAMP01808; (C) Mpro-DRAMP18658; (D) Mpro-DRAMP01342; (E) Mpro-DRAMP01737 and (F) Mpro-DRAMP01771 over the course of 250 ns simulation. Mpro is shown in steel blue color

In Mpro-DRAMP01760 complex, residues HIS41 and ASN142 are interacted for more than 60% of the simulation duration, which helps to establish hydrogen bonds (Figure 4A). Moreover, HIS164, GLU166, GLN189 residues formed various types of H-bonds of same sub-types such as backbone donor, backbone acceptor, side-chain donor, side-chain acceptor, and side-chain donor.[76] A small percentage of ionic interaction in the binding pose has been observed with the residue GLU47. Water bridged interaction with GLN189, ASN142, SER46 in the binding site prevailed during the simulation for more than 40% of time. Furthermore, a small percentage of H-bond and water bridged interactions was also observed in THR25, THR26, and GLY143. Hence, GLN189, ASN142, HIS164, and HIS41 were identified as major interacting residues in the binding of Mpro-DRAMP01760.

In complex Mpro-DRAMP01808, hydrogen bond interacted with CYS145, GLU166, ALA191, GLN189 residues (Figure 4B). In addition, GLN189 contributed more than 60% interaction with peptide. However, the most frequently seemed interactions were hydrophobic and water bridges. It might be because of the presence of a number of hydrophobic, polar and positive residues in the peptide DRAMP01808. In case of hydrophobic interactions, residues HIS41, MET49, LEU50, MET165 interacted more than 30% and HIS164 interacted with a small percentage of 20%. Again, water-bridged contacts with residues THR25, GLN189, HIS41 showed more than 30% longevity.

GLU166 appeared to be a crucial residue to involve in Mpro-DRAMP018658 complexes, with four noncovalent interactions fractions over the residues (Figure 4C). Besides, THR26 seemed to be interacted with a minimal contribution of H-bond. Throughout the simulation, the hydrogen bond and water-bridge interactions were dominant over all other interactions, connecting more than 100% of the time. Presence of different polar and positive residues in the peptide and formation of vital interactions of same subtypes could be among the prime reasons behind this occurrence.[76]

The residue interactions of Mpro-DRAMP01342 were retrieved from a 250 ns simulation trajectory and were classified as hydrogen bond, hydrophobic, ionic and water bridges (Figure 4D). Hydrogen bonding and water bridges interaction with residues seemed most frequent compared to the other interactions. Hydrogen bond with residues THR26, HIS41, ASN142 persisted for more than 75% of the time while THR25, CYS145, GLU166, GLN189 seemed to loosen from the docked pose within a short period of time. Similarly, for water

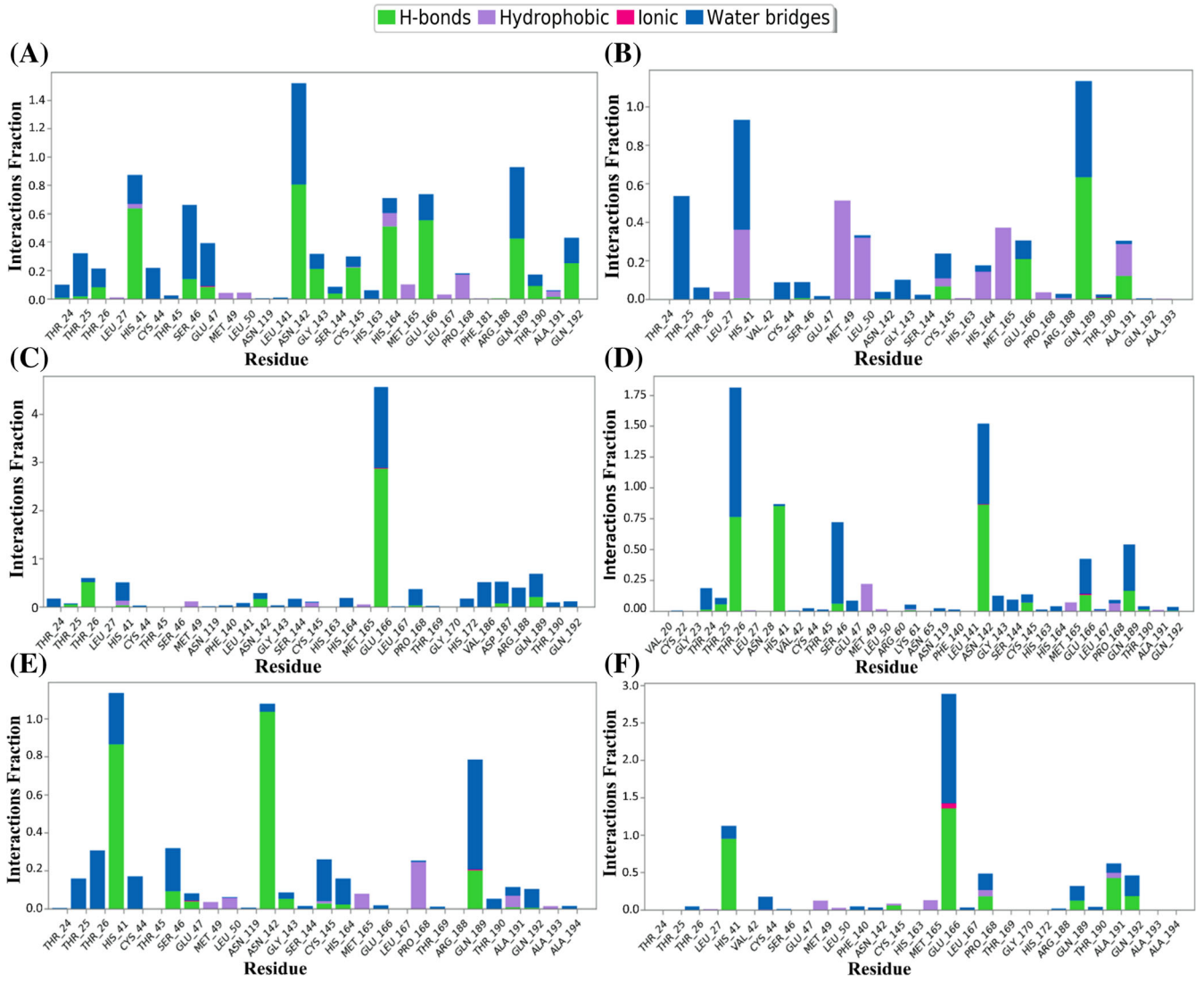

FIGURE 4 Histogram depicts the six Mpro-peptide complexes nonbonded interactions during 250 ns simulation; where the green, purple, pink & blue color represent hydrogen bond, hydrophobic bond, ionic bond and water bridges respectively. (A) Mpro-DRAMP01760; (B) Mpro-DRAMP01808; (C) Mpro-DRAMP018658; (D) Mpro-DRAMP01342; (E) Mpro-DRAMP01737 and (F) Mpro-DRAMP01771

bridge interactions same residue THR26 lasted for about 100%. One study reported that water bridges are assisted to stabilize the Mpro and inhibitor complex structures.[77] MET49 andMET165 seemed frequent with hydrophobic interactions.

The substantial hydrogen bond observed with residue ASN142 in Mpro-DRAMP01737 was retained for more than 100%, emphasizing the fact that the peptide DRAMP01737's initial docked pose did not change during the MD simulation (Figure 4E). Interactions with HIS41 can be classified into two types: H-bond and water-bridges, and it was founded that the interaction with H-bond was stronger (continuing for more than 80%) compared to water-bridges. Hydrophobic and ionic interactions seemed less common with the residues in this complex, though PRO168 seemed moderately connected with hydrophobic interactions. Further, GLU47 and GLN189 found to be interacting with both ionic, water-bridges and H-bond. Additionally, CYS145 seemed to be anchored with water-bridges, H-bond and tiny portion of hydrophobic interactions.

In comparison with previous Mpro-peptide complexes, Mpro-DRAMP01771 implied a different finding in terms of ionic bond interaction (Figure 4F). Ionic interaction with GLU166 proceeded for about 10% in this complex during the simulation period. Furthermore, GLU166 is a crucially significant residue in ligand binding to SARS-CoV-2, and altering it to a hydrophobic residue could reduce ligand inhibitory impact.[63] GLU166 found to be more connected with H-bond and water bridges covering more than 100% of the simulation time in both cases. Hydrophobic, H-bond and water-bridged interactions also observed with residues HIS41, MET49, PRO168, GLN189, ALA191. Consequently, interactions of HIS41, GLU166, ASN142, GLN189, THR26 residues observed very repeated in all Simulations which is aligned with the other findings of the study.[77]

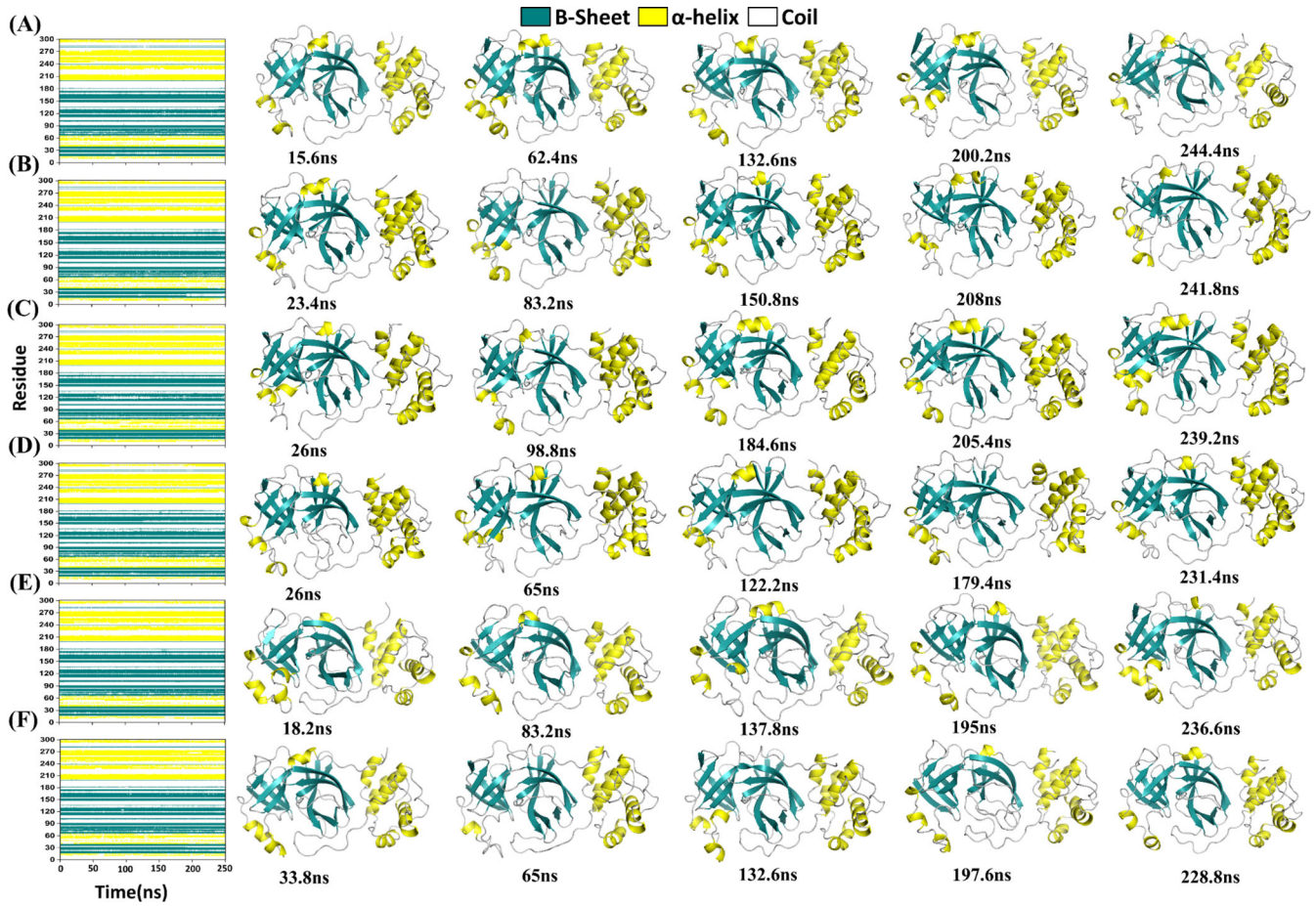

FIGURE 5 Secondary structure composition during entire 250 ns simulation. (A) Mpro-DRAMP01760; (B) Mpro-DRAMP01808; (C) Mpro-DRAMP018658; (D) Mpro-DRAMP01342; (E) Mpro-DRAMP01737 and (F) Mpro-DRAMP01771

3.4 | Protein secondary structure

Protein secondary structure elements (SSE) such as α-helices and β-strands are monitored throughout the DSSP program.[47] SSE analysis of Mpro-DRAMP01760, Mpro-DRAMP01808, Mpro-DRAMP18658, Mpro-DRAMP01342, Mpro-DRAMP01737, Mpro-DRAMP01771 complexes were portrayed respectively (Figure 5). Conformational changes were observed in all protein monomers. The SSE composition of all protein monomers in the trajectory frame fall below 45%, indicating unstructured conformations of protein over the course of the simulation. Residue index demonstrated that Mpro-DRAMP18658 complex displayed 19.11% helix; 25.12% beta strand which comprises of 44.22% of total SSE. However, Mpro-DRAMP01771 contributes a minimal 16.21% helix and 24.72% beta strand showing 40.93% total of SSE. Residues and SSE assignment for protein in peptide-Mpro complexes over the simulation time were also analyzed. In Mpro-DRAMP01760, Mpro-DRAMP01808, Mpro-DRAMP018658, Mpro-DRAMP01342, Mpro-DRAMP01737, and Mpro-DRAMP01771 complex correspondingly, residues of Mpro from 46 to 49, 11 to 16, 10 to 13, 40 to 41, and 46 to 50 revealed the coil structure at various time points during the simulation (Figure 5A–F). However, α-helix containing residues ranges from 11 to14 showed twisted form in Figure 5C.The shape of β-Sheets in Figure 5A was slightly distorted during the simulation.

3.5 | Free energy landscape

Free energy landscape was performed for understanding the relationships between different conformations, transition pathways, energy barriers corresponding to the stability of protein-peptide complex underneath their interaction over the time scale.[78] The weak and unstable interaction of protein-peptide shows multiple energy minimum clusters as they have noticeable energy barriers between their sub-state conformations. However, strong and stable interaction form single energy cluster due to have less energy barriers among their sub-state conformations.[79] The stable configuration with the least amount of energy is represented by deep valleys on a plot, whereas intermediate conformations are represented by the boundaries between deep valleys. The system is thought to reach quasi equilibrium within the valley.[80] Figure 6

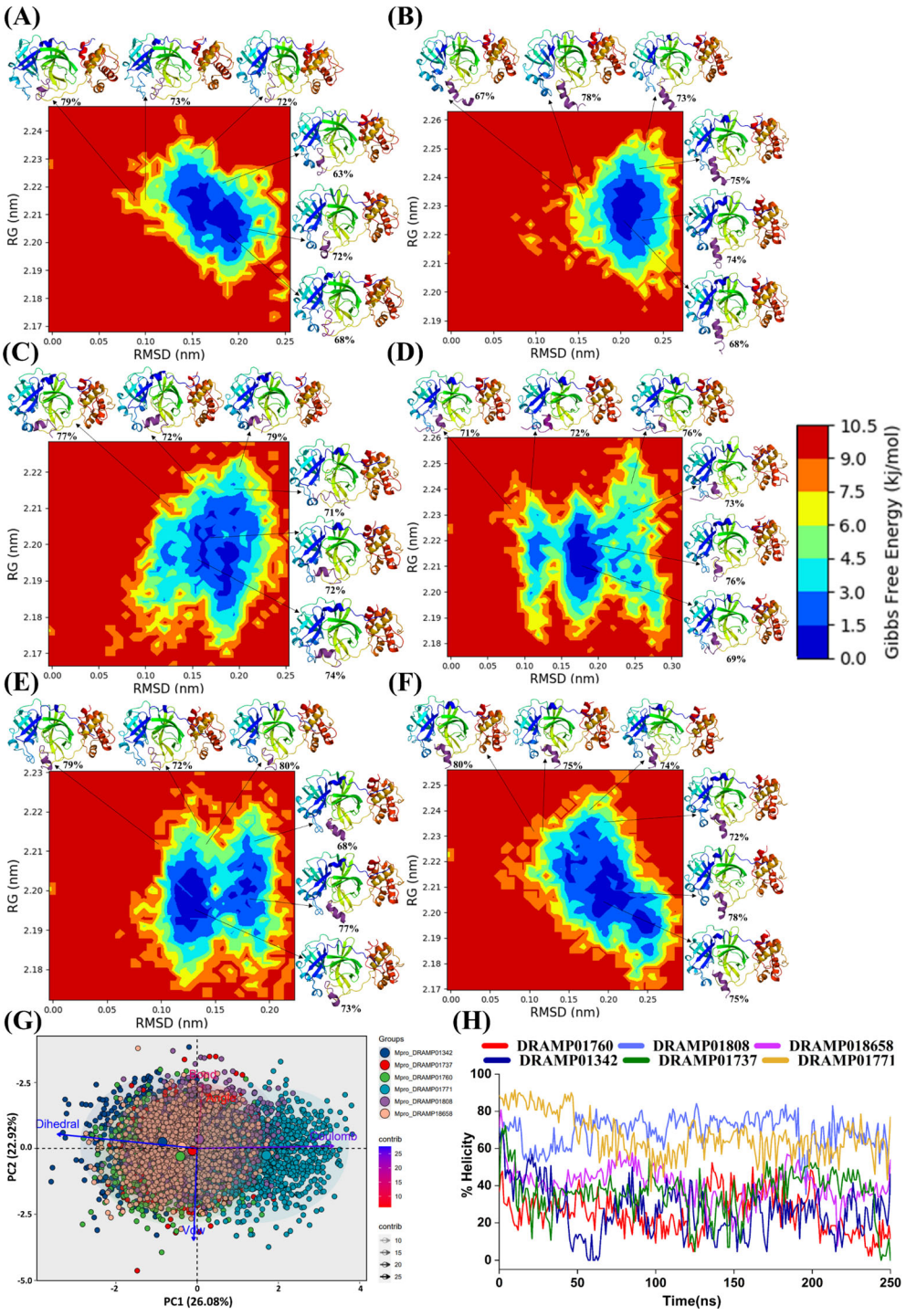

FIGURE 6 Free energy landscapes 2D plot with representative structures of (A) Mpro-DRAMP01760; (B) Mpro-DRAMP01808; (C) Mpro-DRAMP018658; (D) Mpro-DRAMP01342; (E) Mpro-DRAMP01737 and (F) Mpro-DRAMP01771; (G) The principal component analysis plot of Mpro-peptide complexes; (H) Percentage of helix content over 250 ns simulation

depicts the energy minima basins from red to blue, with red denoting less stable conformation with higher energy conformational state and blue denoting more stable conformation with lower energy conformational state. Conformational clustering analysis of FEL indicated that Mpro-DRAMP18658, Mpro-DRAMP01342, Mpro-DRAMP01737, Mpro-DRAMP01771 have multiple energy minimum clusters while Mpro-DRAMP01760, Mpro-DRAMP01808, and Mpro-DRAMP01342 have only one noticeable energy minimum cluster with dark blue areas. Moreover, Mpro-DRAMP01760, Mpro-DRAMP01342, and Mpro-DRAMP01808 also show higher concentrated dark blue areas with minimal energy (Figure 6A,B,D). These observations suggest that the conformational dynamics were less in Mpro-DRAMP18658, Mpro-DRAMP01737, Mpro-DRAMP01771 compared to Mpro-DRAMP01760, Mpro-DRAMP01342, and Mpro-DRAMP01808.[81] Furthermore, representative snapshots exhibiting minimum FEL energy reveal that Mpro-DRAMP01771, Mpro-DRAMP018658, Mpro-DRAMP01737, Mpro-DRAMP01342,

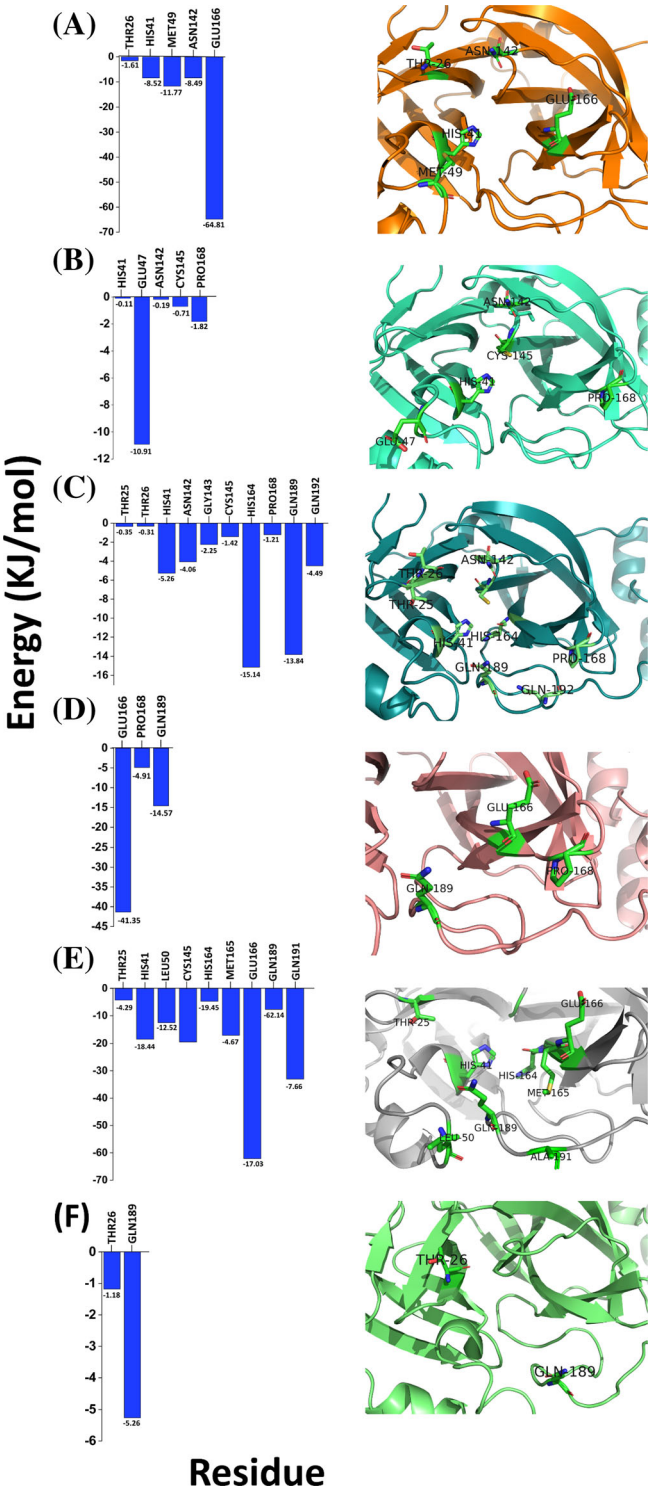

FIGURE 7 Interacting per residue energy contributions of Mpro in Mpro-peptide complex. (A) Mpro-DRAMP01342; (B) Mpro-DRAMP01737; (C) Mpro-DRAMP01760; (D) Mpro-DRAMP01771; (E) Mpro-DRAMP01808 and (F) Mpro-DRAMP18658. Crucial residues of Mpro with preferential binding energy were displayed as stick representations.

Mpro-DRAMP01760, and Mpro-DRAMP01808 have native content of 75%, 74%, 73%, 69%, and 68%, respectively.

3.6 | Principal component analysis and helicity percentage content

Principal component analysis is used to explain the energy and structural properties of six proteins-peptide complexes obtained from MD simulation. The distribution of clusters obtained from the PCA is shown in Figure 6G. The two PCs describe 49% of the variance where PC1 and PC2 cover 22.92% and 26.08% of variance, respectively. It is observed from the score plot that Mpro-DRAMP01737, Mpro-DRAMP01760, Mpro-DRAMP01808, Mpro-DRAMP18658 are overlapped with each other without any significant separation. Thus, the structural and energy profiles are almost unchanged for these protein-peptide complexes as well as these peptides show similar types of binding behavior. The cluster of Mpro-DRAMP01342 shifted upward in the PC2 direction indicating the contribution of bond and bond angle was higher than that of other complexes. The cluster of Mpro-DRAMP01808 shifted slightly to the left and the contribution of dihedral and van der waals energy of Mpro-DRAMP01808 was higher than that of other complexes (Figure S1). Furthermore, score plot displayed that the energy distribution of the five protein-peptide complexes are wider due to the fluctuating nature of the complexes during simulation period. Mpro-DRAMP01771 complex shifted significantly toward the positive direction of PC1 and this indicates a greater dissimilarity of Mpro-DRAMP01771 complex with other complexes. The score plot of PCA reveals that the columbic force shows a positive correlation with the DRAMP01771 complex and was higher than that of other complexes. Therefore, the protein structure is significantly changed due to the binding of DRAMP01771 and Columbic interactions may play a crucial role.

Protein folding, enzyme function and peptide-based drug discovery all are benefited from understanding peptide secondary structure. The biological activities of α-helical AMPs are heavily influenced by their helicity.[82] The percentage of helicity of peptides in the peptide-Mpro complexes was obtained from the analysis of simulation trajectory. Here, DRAMP01760, DRAMP01808, DRAMP18658, DRAMP01342, DRAMP01737, DRAMP01771 show average helicity of 26.98%, 62.22%, 41.41%, 21.78%, 34.57%, and 53.93% respectively during molecular dynamic simulations. Figure 6H displayed that DRAMP01342 has lower percentage of helicity than the other peptides throughout the simulation period due to a distortion of the helical structure away from the ideal a-helix geometry. On the contrary, DRAMP01808 revealed higher percentage helicity than the other peptides.

3.7 | Binding free energy analysis of interacting residues

MM-PBSA per residue free energy decomposition analysis was performed for all complexes to identify the amino acid residues of Mpro with significant interactions with the peptides. It is seen that polar solvation energy opposes the binding but is compensated by van der Waal's energy, electrostatic energy and nonpolar solvation energy.[7] Those amino acid residues contributed to the MM-PBSA binding

energy with negative energy values, and positive energy values are identified as preferential and poor contact residues.[57] Figure 7 depicts the per-residue energy contributions of Mpro in the Mpro-Peptide complexes. With regard to DRAMP01342, five interacting residues showed favorable binding with negative energy namely THR26, HIS41, MET49, ASN142, and GLU166 consequently. In the case of DRAMP01737, HIS41, GLU47, ASN142, CYS145, and PRO168 were demonstrated as the five interfacing residues with favorable binding. Although their contribution was very minimal. As for DRAMP01760, 10 interacting residues exhibited favorable binding with negative energy including THR25, THR26, HIS41, ASN142, GLY143, CYS145, HIS164, PRO168, GLN189, and GLN192 respectively. There were only 3 residues in DRAMP01771 that showed favorable binding energy, whose were GLU166, PRO168, and GLN189 respectively. In the instance of DRAMP01808, nine interacting residues that exhibited preferential binding with negative energy were THR25, HIS41, LEU50, CYS145, HIS164, MET165, GLU166, GLN189, and ALA191 subsequently. Only two interacting residues in DRAMP18658 demonstrated favorable interaction with negative energy: THR26 and GLN189.These findings imply that binding is more preferable and significant in the cases of DRAMP01808 and DRAMP01760 than the other four peptides.[83] These observations also resemble the earlier mentioned FEL data in terms of stability. Consequently, the MM-PBSA study revealed that the previously recognized crucial binding residues HIS41, GLU166, ASN142, GLN189, and THR26 in Mpro were conducive to the binding of Mpro-Peptide complexes. Moreover, the energy profile of interacting residues of peptide in peptide-Mpro complex was displayed in Figure S2. Notably, LYS7, PHE2, PHE1, ARG11, PHE1, PHE1 residues were shown to be thermodynamically favorable for the binding process in DRAMP01342, DRAMP01737, DRAMP01760, DRAMP01771, DRAMP01808, and DRAMP18658, respectively.

4 | CONCLUSIONS

As the present pandemic is driven by a highly contagious new coronavirus, multiple treatment approaches must be developed as quickly as possible. Repurposing of existing antiviral peptides to treat SARS-CoV-2 is a promising therapeutic development method. Mpro SARS CoV-2 may be inhibited by a broad peptide's interface. Our study revealed that six peptides out of two thousand seven hundred eight have ranked top against Mpro based on docking analysis. According to simulation, the intermolecular interactions of these peptides with Mpro are highly dominated by hydrogen bonds. In addition, the residues CYS145, HIS41, PRO168, GLU166, GLN189, ASN142, MET49, and THR26 are important contributors of peptide binding to Mpro of SARS-CoV-2. The (FEL) implies that DRAMP01808, DRAMP01760, and DRAMP01342 have better binding stability. DRAMP01808 is better than DRAMP01760 in percentage helicity content. Conclusively, molecular dynamics simulation results and further comprehensive analysis suggest that DRAMP01808 and DRAMP01760 could be best peptide inhibitor of Mpro. Furthermore, these proposed peptides will be improved by designing peptidomimetic analogs using stapling and assessing their inhibition efficiency by protease inhibition and cell-based luminescent assays.

ACKNOWLEDGMENTS

We are grateful to our donors who supported to build a computational platform (http://grc-bd.org/donate/). The authors like to acknowledge the World Academy of Science (TWAS) to purchase High-Performance Computer for performing molecular dynamics simulation. We are also thankful to Md Shazzadul Islam, Pranta Sarkar, Shariar Iqbal, Borhan Uddin for assisting us in large scale peptide screening against Mpro. Graphical abstract was created with BioRender.com.

CONFLICT OF INTEREST

The authors declare no conflicts of interest.

DATA AVAILABILITY STATEMENT

The data that support the findings of this study are available from the corresponding author upon reasonable request.

ORCID

Mohammad A. Halim https://orcid.org/0000-0002-1698-7044

REFERENCES

[1] *Lancet Infect. Dis.* **2020**, *20*, e215.
[2] C. Huang, Y. Wang, X. Li, L. Ren, J. Zhao, Y. Hu, L. Zhang, G. Fan, J. Xu, X. Gu, Z. Cheng, T. Yu, J. Xia, Y. Wei, W. Wu, X. Xie, W. Yin, H. Li, M. Liu, Y. Xiao, H. Gao, L. Guo, J. Xie, G. Wang, R. Jiang, Z. Gao, Q. Jin, J. Wang, B. Cao, *Lancet* **2020**, *395*, 497.
[3] N. Zhu, D. Zhang, W. Wang, X. Li, B. Yang, J. Song, X. Zhao, B. Huang, W. Shi, R. Lu, P. Niu, F. Zhan, X. Ma, D. Wang, W. Xu, G. Wu, G. F. Gao, W. Tan, *N. Engl. J. Med.* **2020**, *382*, 727.
[4] A. E. Gorbalenya, S. C. Baker, R. S. Baric, R. J. de Groot, C. Drosten, A. A. Gulyaeva, B. L. Haagmans, C. Lauber, A. M. Leontovich, B. W. Neuman, D. Penzar, S. Perlman, L. L. M. Poon, D. V. Samborskiy, I. A. Sidorov, I. Sola, J. Ziebuhr, C. S. G. of the I. C. on T. of Viruses, *Nat. Microbiol.* **2020**, *5*, 536.
[5] L. Zhang, D. Lin, X. Sun, U. Curth, C. Drosten, L. Sauerhering, S. Becker, K. Rox, R. Hilgenfeld, *Science (80-.)* **2020**, *368*, 409. https://doi.org/10.1126/science.abb3405
[6] R. Hilgenfeld, C. R. Hilgenfeld, *FEBS J.* **2014**, *281*, 4085.
[7] J. Yang, X. Lin, N. Xing, Z. Zhang, H. Zhang, H. Wu, W. Xue, *J. Chem. Inf. Model.* **2021**, *61*, 3917.
[8] C. A. Ramos-Guzmán, J. J. Ruiz-Pernía, I. Tuñón, *ACS Catal.* **2020**, *10*, 12544.
[9] L. Silvestrini, N. Belhaj, L. Comez, Y. Gerelli, A. Lauria, V. Libera, P. Mariani, P. Marzullo, M. G. Ortore, A. Palumbo Piccionello, C. Petrillo, L. Savini, A. Paciaroni, F. Spinozzi, *Sci. Rep.* **2021**, *11* ,409. https://doi.org/10.1038/s41598-021-88630-9
[10] W. Vuong, M. B. Khan, C. Fischer, E. Arutyunova, T. Lamer, J. Shields, H. A. Saffran, R. T. McKay, M. J. van Belkum, M. A. Joyce, H. S. Young, D. L. Tyrrell, J. C. Vederas, M. J. Lemieux, *Nat. Commun.* **2020**, *11*, 4282. https://doi.org/10.1038/s41467-020-18096-2
[11] T. Pillaiyar, M. Manickam, V. Namasivayam, Y. Hayashi, S.-H. Jung, *J. Med. Chem.* **2016**, *59*, 6595.
[12] Z. Jin, X. Du, Y. Xu, Y. Deng, M. Liu, Y. Zhao, B. Zhang, X. Li, L. Zhang, C. Peng, Y. Duan, J. Yu, L. Wang, K. Yang, F. Liu, R. Jiang, X. Yang, T. You, X. Liu, X. Yang, F. Bai, H. Liu, X. Liu, L. W. Guddat, W. Xu, G.

Xiao, C. Qin, Z. Shi, H. Jiang, Z. Rao, H. Yang, *Nature* **2020**, *582*, 289. https://doi.org/10.1038/s41586-020-2223-y
[13] Z. Jin, Y. Zhao, Y. Sun, B. Zhang, H. Wang, Y. Wu, Y. Zhu, C. Zhu, T. Hu, X. Du, Y. Duan, J. Yu, X. Yang, X. Yang, K. Yang, X. Liu, L. W. Guddat, G. Xiao, L. Zhang, H. Yang, Z. Rao, *Nat. Struct. Mol. Biol.* **2020**, *27*, 529. https://doi.org/10.1038/s41594-020-0440-6
[14] T. Pillaiyar, *Med. Chem. (Los. Angeles)* **2015**, *5*, 361. https://doi.org/10.4172/2161-0444.1000287
[15] B. Goyal, D. Goyal, *ACS Comb. Sci.* **2020**, *22*, 297.
[16] D. R. Owen, C. M. N. Allerton, A. S. Anderson, L. Aschenbrenner, M. Avery, S. Berritt, B. Boras, R. D. Cardin, A. Carlo, K. J. Coffman, A. Dantonio, L. Di, H. Eng, R. A. Ferre, K. S. Gajiwala, S. A. Gibson, S. E. Greasley, B. L. Hurst, E. P. Kadar, A. S. Kalgutkar, J. C. Lee, J. Lee, W. Liu, S. W. Mason, S. Noell, J. J. Novak, R. S. Obach, K. Ogilvie, N. C. Patel, M. Pettersson, D. K. Rai, M. R. Reese, M. F. Sammons, J. G. Sathish, R. S. P. Singh, C. M. Steppan, A. E. Stewart, J. B. Tuttle, L. Updyke, P. R. Verhoest, L. Wei, Q. Yang, Y. Zhu, *Science (80-.)* **2021**, *374*, 1586. https://doi.org/10.1126/SCIENCE.ABL4784/SUPPL_FILE/SCIENCE.ABL4784_MDAR_REPRODUCIBILITY_CHECKLIST.PDF
[17] J. Johansen-Leete, S. Ullrich, S. E. Fry, R. Frkic, M. J. Bedding, A. Aggarwal, A. S. Ashhurst, K. B. Ekanayake, M. C. Mahawaththa, V. M. Sasi, S. Luedtke, D. J. Ford, A. J. O'Donoghue, T. Passioura, M. Larance, G. Otting, S. Turville, C. J. Jackson, C. Nitsche, R. J. Payne, *Chem. Sci.* **2022**, *13*, 3826. https://doi.org/10.1039/D1SC06750H
[18] M. Muttenthaler, G. F. King, D. J. Adams, P. F. Alewood, *Nat. Rev. Drug Discov.* **2021**, *20*, 309. https://doi.org/10.1038/s41573-020-00135-8
[19] I. D'Annessa, F. S. Di Leva, A. La Teana, E. Novellino, V. Limongelli, D. Di Marino, *Front. Mol. Biosci.* **2020**, *7*, 1.
[20] K. Fosgerau, T. Hoffmann, *Drug Discov. Today* **2015**, *20*, 122.
[21] L. J. Zhang, R. L. Gallo, *Curr. Biol.* **2016**, *26*, R14. https://doi.org/10.1016/j.cub.2015.11.017
[22] K. L. Brown, R. E. W. Hancock, *Curr. Opin. Immunol.* **2006**, *18*, 24. https://doi.org/10.1016/j.coi.2005.11.004
[23] S. Elnagdy, M. Alkhazindar, *ACS Pharmacol. Transl. Sci.* **2020**, *3*, 780. https://doi.org/10.1021/ACSPTSCI.0C00059
[24] D. J. Craik, D. P. Fairlie, S. Liras, D. Price, *Chem. Biol. Drug Des.* **2013**, *81*, 136. https://doi.org/10.1111/cbdd.12055
[25] T. Kruse, H. H. Kristensen, *Expert Rev. Anti-infect. Ther.* **2008**, *6*, 887. https://doi.org/10.1586/14787210.6.6.887
[26] J. L. Lau, M. K. Dunn, *Bioorg. Med. Chem.* **2018**, *26*, 2700. https://doi.org/10.1016/j.bmc.2017.06.052
[27] A. G. Kreutzer, M. Krumberger, E. M. Diessner, C. M. T. Parrocha, M. A. Morris, G. Guaglianone, C. T. Butts, J. S. Nowick, *Eur. J. Med. Chem.* **2021**, *221*, 113530. https://doi.org/10.1016/J.EJMECH.2021.113530
[28] P. M. Mishra, C. K. Nandi, *J. Phys. Chem. B* **2021**, *125*, 8395. https://doi.org/10.1021/ACS.JPCB.1C03294/SUPPL_FILE/JP1C03294_SI_001.PDF
[29] B. D. Kevadiya, J. Machhi, J. Herskovitz, M. D. Oleynikov, W. R. Blomberg, N. Bajwa, D. Soni, S. Das, M. Hasan, M. Patel, A. M. Senan, S. Gorantla, J. E. McMillan, B. Edagwa, R. Eisenberg, C. B. Gurumurthy, S. P. M. Reid, C. Punyadeera, L. Chang, H. E. Gendelman, *Nat. Mater.* **2021**, *2021*, 205.
[30] T. U. Singh, S. Parida, M. C. Lingaraju, M. Kesavan, D. Kumar, R. K. Singh, *Pharmacol. Rep.* **2020**, *72*, 1479.
[31] S. Pushpakom, F. Iorio, P. A. Eyers, K. J. Escott, S. Hopper, A. Wells, A. Doig, T. Guilliams, J. Latimer, C. McNamee, A. Norris, P. Sanseau, D. Cavalla, M. Pirmohamed, *Nat. Rev. Drug Discov.* **2018**, *18*, 41. https://doi.org/10.1038/nrd.2018.168
[32] B. L. Le, G. Andreoletti, T. Oskotsky, A. Vallejo-Gracia, R. Rosales, K. Yu, I. Kosti, K. E. Leon, D. G. Bunis, C. Li, G. R. Kumar, K. M. White, A. García-Sastre, M. Ott, M. Sirota, *Sci. Rep.* **2021**, *11*, 12310. https://doi.org/10.1038/s41598-021-91625-1
[33] S. M. Chowdhury, S. A. Talukder, A. M. Khan, N. Afrin, M. A. Ali, R. Islam, R. Parves, A. Al Mamun, M. A. Sufian, M. N. Hossain, M. A. Hossain, M. A. Halim, *J. Phys. Chem. B* **2020**, *124*, 9785.
[34] F. M. Efaz, S. Islam, S. A. Talukder, S. Akter, M. Z. Tashrif, M. A. Ali, M. A. Sufian, M. R. Parves, M. J. Islam, M. A. Halim, *J. Comput. Chem.* **2021**, *42*, 2283. https://doi.org/10.1002/jcc.26758
[35] M. M. H. Sakib, A. A. Nishat, M. T. Islam, M. A. Raihan Uddin, M. S. Iqbal, F. F. Bin Hossen, M. I. Ahmed, M. S. Bashir, T. Hossain, U. S. Tohura, S. I. Saif, N. R. Jui, M. Alam, M. A. Islam, M. M. Hasan, M. A. Sufian, M. A. Ali, R. Islam, M. A. Hossain, M. A. Halim, *Comput. Biol. Med.* **2021**, *136*, 104759. https://doi.org/10.1016/j.compbiomed.2021.104759
[36] G. Shi, X. Kang, F. Dong, Y. Liu, N. Zhu, Y. Hu, H. Xu, X. Lao, H. Zheng, *Nucleic Acids Res.* **2022**, *50*, D488.
[37] L. Fan, J. Sun, M. Zhou, J. Zhou, X. Lao, H. Zheng, H. Xu, *Sci. Rep.* **2016**, *2016*, 61.
[38] A. Lamiable, P. Thévenet, J. Rey, M. Vavrusa, P. Derreumaux, P. Tufféry, *Nucleic Acids Res.* **2016**, *44*, W449.
[39] J. Maupetit, P. Derreumaux, P. Tuffery, *Nucleic Acids Res.* **2009**, *37*, W498.
[40] D. Schneidman-Duhovny, Y. Inbar, R. Nussinov, H. J. Wolfson, *Nucleic Acids Res.* **2005**, *33*, W363.
[41] N. Andrusier, R. Nussinov, H. J. Wolfson, *Proteins* **2007**, *69*, 139. https://doi.org/10.1002/prot.21495
[42] P. Mark, L. Nilsson, *J. Phys. Chem. A* **2001**, *105*, 9954. https://doi.org/10.1021/jp003020w
[43] K. J. Bowers, F. D. Sacerdoti, J. K. Salmon, Y. Shan, D. E. Shaw, E. Chow, H. Xu, R. O. Dror, M. P. Eastwood, B. A. Gregersen, J. L. Klepeis, I. Kolossvary, M. A. Moraes, Proceedings of the 2006 ACM/-IEEE conference on Supercomputing - SC '06; 2006ACM Press, New York, USA, **2006**.
[44] A. Allouche, *J. Comput. Chem.* **2011**, *32*, 174. https://doi.org/10.1002/jcc.21600
[45] Y. Shan, J. L. Klepeis, M. P. Eastwood, R. O. Dror, D. E. Shaw, *J. Chem. Phys.* **2005**, *122*, 054101. https://doi.org/10.1063/1.1839571
[46] S. J. Stuart, R. Zhou, B. J. Berne, *J. Chem. Phys.* **1996**, *105*, 1426. https://doi.org/10.1063/1.472005
[47] W. Kabsch, C. Sander, *Biopolymers* **1983**, *22*, 2577. https://doi.org/10.1002/bip.360221211
[48] Y. Wang, R. Gu, H. Fan, J. Ulmschneider, D. Wei, *Adv. Exp. Med. Biol.* **2015**, *827*, 71. https://doi.org/10.1007/978-94-017-9245-5_6
[49] L. P. Kagami, G. M. das Neves, L. F. S. M. Timmers, R. A. Caceres, V. L. Eifler-Lima, *Comput. Biol. Chem.* **2020**, *87*, 107322. https://doi.org/10.1016/j.compbiolchem.2020.107322
[50] I. Multivariate, *Data Handl. Sci. Technol.* **1998**, *20*, 349. https://doi.org/10.1016/S0922-3487(98)80046-4
[51] R. Vidal, Y. Ma, S. S. Sastry, *Interdiscip. Appl. Math.* **2016**, *40*, 25. https://doi.org/10.1007/978-0-387-87811-9_2
[52] M. J. Islam, A. M. Khan, M. R. Parves, M. N. Hossain, M. A. Halim, *Sci. Rep.* **2019**, *9*, 16426. https://doi.org/10.1038/s41598-019-52308-0
[53] D. Greene, W. M. Botello-Smith, A. Follmer, L. Xiao, E. Lambros, R. Luo, *J. Phys. Chem. B* **2016**, *20*, 12293. https://doi.org/10.1021/ACS.JPCB.6B09535/SUPPL_FILE/JP6B09535_SI_001.PDF
[54] J. F. Varughese, T. Baxley, J. M. Chalovich, Y. Li, *J. Phys. Chem. B* **2011**, *115*, 2392. https://doi.org/10.1021/JP1094504/ASSET/IMAGES/MEDIUM/JP-2010-094504_0011.GIF
[55] C. Wang, P. H. Nguyen, K. Pham, D. Huynh, T. B. N. Le, H. Wang, P. Ren, R. Luo, *J. Comput. Chem.* **2016**, *37*, 2436. https://doi.org/10.1002/JCC.24467
[56] Y. Zhang, Q. C. Zheng, *J. Theor. Biol.* **2018**, *447*, 118. https://doi.org/10.1016/J.JTBI.2018.03.028
[57] A. Gupta, N. Chaudhary, P. Aparoy, *Int. J. Biol. Macromol.* **2018**, *119*, 352. https://doi.org/10.1016/J.IJBIOMAC.2018.07.050
[58] R. Kumari, R. Kumar, A. Lynn, *J. Chem. Inf. Model.* **2014**, *54*, 1951. https://doi.org/10.1021/CI500020M/SUPPL_FILE/CI500020M_SI_001.PDF

[59] M. Paloni, C. Cavallotti, *ACS Omega* **2017**, *2*, 6464. https://doi.org/10.1021/ACSOMEGA.7B01123/ASSET/IMAGES/AO-2017-011235_M002.GIF
[60] S. Kannan, M. R. Pradhan, J. Cherian, T. L. Joseph, Z. Y. Poh, Y. Hai Yan, H. Melvyn, L. Boping, H. Jeffrey, K. Nacro, C. S. Verma, *ACS Omega* **2017**, *2*, 7881. https://doi.org/10.1021/ACSOMEGA.7B01403/ASSET/IMAGES/LARGE/AO-2017-01403B_0008.JPEG
[61] M. Aldeghi, M. J. Bodkin, S. Knapp, P. C. Biggin, *J. Chem. Inf. Model.* **2017**, *57*, 2203. https://doi.org/10.1021/ACS.JCIM.7B00347/ASSET/IMAGES/CI-2017-003475_M033.GIF
[62] C. N. Patel, S. P. Jani, D. G. Jaiswal, S. P. Kumar, N. Mangukia, R. M. Parmar, R. M. Rawal, H. A. Pandya, *Sci. Rep.* **2021**, *2021*, 111.
[63] S. T. Ngo, N. Q. A. Pham, L. T. Le, D. H. Pham, V. V. Vu, *J. Chem. Inf. Model.* **2020**, *60*, 5771. https://doi.org/10.1021/ACS.JCIM.0C00491/SUPPL_FILE/CI0C00491_SI_002.MPG
[64] C. Pedebos, S. Khalid, *Nat. Rev. Microbiol.* **2022**, *20*, 192.
[65] Y. Zhang, J. Skolnick, *J. Comput. Chem.* **2004**, *25*, 865. https://doi.org/10.1002/jcc.20011
[66] T. Meyer, M. D'abramo, A. Hospital, M. Rueda, C. Ferrer-Costa, A. Pé Rez, O. Carrillo, J. Camps, C. Fenollosa, D. Repchevsky, J. Lluis Gelpí, M. Orozco, *Struct. Des.* **2010**, *18*, 1399. https://doi.org/10.1016/j.str.2010.07.013
[67] L. Ivanova, J. Tammiku-Taul, A. T. García-Sosa, Y. Sidorova, M. Saarma, M. Karelson, *ACS Omega* **2018**, *3*, 11407. https://doi.org/10.1021/ACSOMEGA.8B01524/SUPPL_FILE/AO8B01524_SI_001.PDF
[68] J. Akachar, C. Etchebest, R. El Jaoudi, A. Ibrahimi, *Sci. Rep.* **2021**, *2021*, 111.
[69] D. Zhang, R. Lazim, *Sci. Rep.* **2017**, *2017*, 71.
[70] T. J. Stevens, I. T. Arkin, *Proteins* **1999**, *36*, 135. https://doi.org/10.1002/(SICI)1097-0134(19990701)36:1
[71] G. D. Rose, A. R. Geselowitz, G. J. Lesser, R. H. Lee, M. H. Zehfus, *Science (80-.)* **1985**, *229*, 834. https://doi.org/10.1126/SCIENCE.4023714
[72] S. Doniach, P. Eastman, *Curr. Opin. Struct. Biol.* **1999**, *9*, 157. https://doi.org/10.1016/S0959-440X(99)80022-0
[73] R. K. Tiwari, R. P. Ojha, G. Tiwari, V. Pandey, V. Mall, *AIP Conf. Proc.* **2018**, *1953*, 130030. https://doi.org/10.1063/1.5033174
[74] A. Kumari, V. S. Rajput, P. Nagpal, H. Kukrety, S. Grover, A. Grover, *J. Biomol. Struct. Dyn.* **2020**, *40*, 4987. https://doi.org/10.1080/07391102.2020.1864476/SUPPL_FILE/TBSD_A_1864476_SM8485.PDF
[75] I. Aier, P. K. Varadwaj, U. Raj, *Sci. Rep.* **2016**, *2016*, 61.
[76] M. I. Choudhary, M. Shaikh, *PLoS One* **2020**, *15*,e0235030. https://doi.org/10.1371/JOURNAL.PONE.0235030
[77] R. Yoshino, N. Yasuo, M. Sekijima, *Sci. Rep.* **2020**, *2020*, 101.
[78] S. Gupta, A. K. Singh, P. P. Kushwaha, K. S. Prajapati, M. Shuaib, S. Senapati, S. Kumar, *J. Biomol. Struct. Dyn.* **2021**, *39*, 4334. https://doi.org/10.1080/07391102.2020.1776157
[79] C. B. Mishra, P. Pandey, R. D. Sharma, M. Z. Malik, R. K. Mongre, A. M. Lynn, R. Prasad, R. Jeon, A. Prakash, *Brief. Bioinform.* **2021**, *22*, 1346.
[80] M. T. Khan, A. Khan, A. U. Rehman, Y. Wang, K. Akhtar, S. I. Malik, D. Q. Wei, *Sci. Rep.* **2019**, *9*, *1*. https://doi.org/10.1038/s41598-019-44013-9
[81] A. C. Bharathi, P. K. Yadav, B. Syed Ibrahim, *Mol. BioSyst.* **2016**, *12*, 1128. https://doi.org/10.1039/C5MB00786K
[82] T. Tian, W. Xie, L. Liu, S. Fan, H. Zhang, Z. Qin, C. Yang, *Crit. Rev. Food Sci. Nutr.* **2021**, 1. https://doi.org/10.1080/10408398.2021.2019673
[83] Z. Xiao, Y. Cong, K. Huang, S. Zhong, J. Z. H. Zhang, L. Duan, *Phys. Chem. Chem. Phys.* **2019**, *21*, 20951. https://doi.org/10.1039/C9CP02851J

SUPPORTING INFORMATION

Additional supporting information can be found online in the Supporting Information section at the end of this article.

How to cite this article: M. J. Uddin, H. Akhter, U. Chowdhury, J. Mawah, S. T. Karim, M. Jomel, M. S. Islam, M. R. Islam, L. A. B. Onin, M. A. Ali, F. M. Efaz, M. A. Halim, *J. Comput. Chem.* **2022**, 1. https://doi.org/10.1002/jcc.27050